Nucleation rates and induction times during colloidal crystallization: Links between models and experiments

Narendra M. Dixit and Charles F. Zukoski*
Department of Chemical Engineering, University of Illinois at Urbana-Champaign, 114, Roger Adams Laboratory, 600 South Mathews Avenue, Urbana, Illinois 61801

(Received 22 March 2002; revised manuscript received 12 July 2002; published 11 November 2002)

A kinetic model for the evolution of the cluster size distribution during crystal nucleation and growth is presented. The model allows one to establish precise links between model parameters and experimental measures of nucleation kinetics. This approach demonstrates the significance of several processes not accounted for in classical nucleation theories. Chief among these is that the driving force for crystal nucleation decreases rapidly due to a reduction of the background monomer concentration as crystallization progresses, resulting in a reduction of nucleation rates. This, coupled with the disparities in the definitions of measured and predicted quantities, leads to significant discrepancies between predictions of extant models and experimental estimates of nucleation rates. Accounting for these effects, calculations of the kinetic model are shown to be in good agreement with experimental estimates of nucleation rates, crystal growth velocities, and induction times during the crystallization of hard sphere colloidal suspensions.

DOI: 10.1103/PhysRevE.66.051602 PACS number(s): 82.70.Dd

I. INTRODUCTION

The kinetics of crystallization of colloidal suspensions has seen extensive study due to the ability of these systems to mimic molecular crystallization and due to applications involving highly ordered arrays of colloidal particles [1–3]. Since the pioneering work of Becker and Doring [4], models based on classical nucleation theory have been employed to analyze nucleation kinetic data [5,6]. Despite being the standard, however, comparisons of experimental estimates of nucleation rates and predictions of classical models are poor, often showing discrepancies of tens of orders of magnitude [5,6]. Experimental investigation of nucleation kinetics in molecular systems is difficult because of the small time and length scales associated with nucleation phenomena in these systems and can be a cause for these discrepancies [5,7]. Colloidal suspensions render these time and length scales amenable to experimental measurement. Even in these systems, however, independent estimates of nucleation rates obtained using different experimental techniques but under identical crystallization conditions show severe discrepancies not only for complex systems such as proteins [8], but also for well characterized hard sphere colloidal suspensions [9,10].

One reason for these discrepancies lies in the inadequacies in the nucleation rate models employed. Due to the focus of classical models on the energetics of cluster formation, a detailed description of what is inherently a nonequilibrium, kinetic process is compromised. Further, uncertainties exist in our knowledge of the solid fluid surface tension—often used as an adjustable parameter—to which predictions of classical nucleation theory are extremely sensitive [5,6,9–12]. As crystallization progresses, the background concentration drops significantly reducing the driving force for subsequent crystallization [8,13,14], whereas extant theories assume the supersaturation to remain constant. For more complex systems such as proteins, discrepancies arise from uncertainties in the knowledge of the pair interactions as well, and these details have not been incorporated into descriptions of nucleation kinetics [15–22].

A second reason for the discrepancies between model predictions and experimental results lies in the disparities between the quantities measured experimentally and the quantities predicted by models. Nucleation rates are determined from light scattering experiments [13,14] where the scattered intensity detected involves the cumulative effect of the distribution of cluster sizes, whereas models predict the nucleation rate of clusters of the critical size (defined below). Estimates of nucleation rates are often obtained by measuring induction times during crystallization [13,14,23–26], usually defined as the time after supersaturating a suspension for detectable crystals to first appear. Links between induction times and nucleation rates are only empirical [8,23,25,27], making comparisons of model predictions and measurable quantities questionable. Currently, no models exist for predicting induction times.

Due to these limitations, definitive interpretations of the data obtained from experiments on the kinetics of crystal nucleation are difficult. As a consequence, a fundamental understanding of the governing principles of the crystallization process is still lacking. To facilitate such an understanding, we present in this paper a model of colloidal crystallization kinetics that predicts precisely the quantities measured in nucleation kinetics experiments.

We consider light scattering experiments on supersaturated hard sphere colloidal suspensions. There are two advantages of starting with this system. First, there is a grow-

*Author to whom all correspondence should be addressed. Email address: czukoski@uiuc.edu

ing database with which to compare our predictions [9,12–14,28–38]. Second, the pair potentials governing the particle interactions are well understood: Two hard sphere particles experience no direct interactions in suspension except for an infinite repulsion at contact. The resulting phase behavior is simple: only solid-fluid phase transitions occur, governed by a single parameter, the particle volume fraction, ϕ [39,40]. The freezing boundary occurs at $\phi_s = 0.495$. As ϕ increases above ϕ_s, an increasing fraction of the suspension is eventually crystallized, the fraction reaching 100% at the melting boundary, $\phi_m = 0.55$. When $\phi > \phi_m$, 100% crystallization is achieved with the crystalline phase at a packing fraction ϕ equal to the initial particle volume fraction in the fluid phase. Crystallization can be suppressed under terrestrial conditions by rapid increases of ϕ above ϕ_s, resulting in a hard sphere glass at $\phi \sim 0.58$ [41]. In microgravity, crystals eventually emerge from glassy suspensions [36].

Light scattering experiments detect the number and the size of the scattering units in a crystallizing sample. Therefore, prediction of quantities derived from these measurements demands knowledge of the evolution of the distribution of cluster sizes as crystallization progresses. Previously, cluster size distributions have been predicted using classical nucleation theory, but the assumptions employed make the predictions approximate [5,42–46]. For example, Wu [42] assumes that a steady state distribution of small clusters is instantaneously achieved, whereas Schneidman and Weinberg [43] assume that small clusters exist in an equilibrium distribution dictated by the energetics of cluster formation. Shi and Seinfeld [44] rigorously calculate the evolution of the distribution of clusters of all sizes, but assume that the background monomer concentration remains fixed as crystallization progresses.

Here, we develop a population balance model to describe the evolution of the cluster size distribution in crystallizing systems. In this model, clusters form and grow as a result of a competition between two processes: the aggregation of single particles onto and the dissociation of single particles from cluster surfaces. Particles aggregate onto cluster surfaces by gradient diffusion, driven by the differences between their concentrations in the bulk suspension and near cluster surfaces. Particles on cluster surfaces reside in potential energy wells because of their bonds with neighboring particles. These surface particles dissociate back into the bulk suspension by diffusing out of their respective potential wells via thermal motion. In a previous study [10], we have developed descriptions of these processes for hard sphere systems and calculated steady state nucleation rates and crystal growth velocities. Here, we employ these descriptions to build a population balance model that allows the determination of the evolution of the cluster size distribution. Interestingly, we find that as crystallization progresses the background monomer volume fraction rapidly decreases from the initial value, lowering the driving force for crystallization significantly. This important effect is ignored in classical approaches. Linking the quantities measured in scattering experiments to the cluster size distribution, we are able to predict the measured nucleation rates, crystal growth velocities, and, in particular, induction times. The predictions are in very good agreement with reported quantities. The model thus provides significant insights into the underlying mechanisms governing crystal nucleation and also a more rigorous route for interpreting data obtained from nucleation kinetics experiments.

The paper is organized as follows. In Sec. II, we describe the quantities measured in scattering experiments in terms of the cluster size distribution in a crystallizing sample. In Sec. III, we develop the population balance model that predicts the time evolution of this cluster size distribution. In Sec. IV, we present model predictions of cluster size distributions and experimental quantities including nucleation rates, crystal growth velocities, and induction times, and compare them with experiments. In Sec. V we draw conclusions.

II. QUANTITIES ESTIMATED FROM LIGHT SCATTERING EXPERIMENTS

We consider a colloidal suspension containing spherical particles of radii a, occupying a volume fraction ϕ_0. If $\phi_0 > \phi_s$, the particles will aggregate to form growing clusters. With time, a distribution of cluster sizes, $n(m,t)$, defined as the number of clusters in the sample containing m monomers at a time t after the onset of crystallization, emerges and the volume fraction of single particles, or monomers, decreases. In typical light scattering experiments [13,14], the intensity of light scattered by such a suspension is detected around the first Bragg peak. As crystals nucleate, the Bragg peak grows and narrows. The area under the Bragg peak contains information about the fraction of the suspension that is crystalline, while the width of the peak contains information of the average crystal size. This information is analyzed to obtain induction times, crystal growth velocities, and nucleation rates [13,14,36]. Below, we use Bragg scattering theory to relate measured quantities to the cluster size distribution, $n(m,t)$.

Using Laue's approximation [47], the linewidth of the scattering from a cubic crystalline cluster consisting of m particles can be shown to equal $1/(2a)m^{1/3}$ and is inversely proportional to the linear dimension of the cubic crystal. Here, $2a$ is the lattice spacing assumed to equal a particle diameter. In the presence of more than one cluster, the linewidth gives an average cluster size. Assuming the clusters to be optically independent so that the total intensity scattered is the sum of the intensities scattered by the individual clusters [47], the average crystal size follows as:

$$\frac{L(t)}{2a} = \frac{\sum_{m=m^*}^{\infty} m^{4/3} f(m,t)}{\sum_{m=m^*}^{\infty} m f(m,t)}, \tag{1}$$

where the smallest sized cluster that can produce a detectable Bragg scattering intensity is set to m^*, the critical cluster size defined below, and $f(m,t) = n(m,t)/N$ is the normalized cluster size distribution, with N being the total number of monomers in the suspension at time $t = 0$ marking the onset of crystallization.

The fraction of the suspension crystallized, $X(t)$, is defined as the ratio of the volume occupied by the crystals to the total volume of the suspension. Assuming that an m particle cluster occupies a spherical volume of radius $R_m \approx a(m/\phi_{\text{cryst}})^{1/3}$, it follows that

$$X(t)=\phi_0 \sum_{m=m^*}^{\infty} \frac{m f(m,t)}{\phi_{\text{cryst}}(\phi(t))}, \tag{2}$$

where ϕ_{cryst} is the packing fraction of monomers inside a cluster, assumed here to be independent of m but dependent on the instantaneous monomer volume fraction, $\phi(t)$. It can be shown that $X(t)$ determined experimentally agrees with Eq. (2) to within a constant multiplicative factor.

Finally, the number density of (average-sized) crystals $N_c(t)$ is calculated as the ratio $X(t)/L^3(t)$ and can be written as

$$N_c(t)=\frac{\phi_0}{(2a)^3\phi_{\text{cryst}}(\phi(t))}\frac{[\Sigma_{m=m^*}^{\infty} m f(m,t)]^4}{[\Sigma_{m=m^*}^{\infty} m^{4/3} f(m,t)]^3}, \tag{3}$$

giving the experimental nucleation rate

$$J(t)=\frac{dN_c(t)}{dt}. \tag{4}$$

Classical theories predict the steady state nucleation rate as the steady rate of increase of clusters bigger than the critical size [5]. Thus, $J_{\text{classical}}$ is proportional to $d[\Sigma_{m=m^*}^{\infty} f(m,t)]/dt$. Clearly, this is not the same as the rate $J(t)$ determined experimentally, the latter representing a substantially different average over the cluster size distribution. Similarly, the crystal growth velocities, dR_m/dt, predicted by models are not the same as the velocities, $dL(t)/dt$, determined experimentally. It is not surprising, therefore, that extant models are poor predictors of measured quantities. To extract meaningful information from these experiments, we require a model that predicts the evolution of the cluster size distribution, $f(m,t)$, the background monomer volume fraction, $\phi(t)$, and the crystal packing fraction, ϕ_{cryst}. We develop such a model in the following section.

III. POPULATION BALANCE MODEL

We consider again a colloidal suspension containing N spherical particles of radii a, occupying a volume fraction $\phi_0 > \phi_s$. In this suspension, individual clusters form and grow as a result of the competition between two processes: the aggregation of monomers onto and the dissociation of monomers from cluster surfaces. The rates of these processes, denoted β and α, respectively, depend on m and ϕ. On average, a cluster grows if $\beta > \alpha$ and shrinks if $\beta < \alpha$. At any ϕ, the size $m^* = m^*(\phi)$ at which $\alpha = \beta$ is called the critical cluster size. Here, $\phi(t) = \nu_p n(1,t)$ and $\nu_p = 4\pi a^3/3$.

When N is large, population balance determines the evolution of the cluster size distribution of the normalized number densities, $f(m,t) = n(m,t)/N$, as

$$\begin{aligned}\frac{df(m,t)}{dt} &= f(m+1,t)\alpha(m+1,\phi) + f(m-1,t)\beta(m-1,\phi) \\ &\quad - f(m,t)[\alpha(m,\phi)+\beta(m,\phi)], \quad m>1, \\ \frac{df(1,t)}{dt} &= 2f(2,t)\alpha(2,\phi) - 2f(1,t)\beta(1,\phi) \\ &\quad + \sum_{m=2}^{\infty}[f(m+1,t)\alpha(m+1,\phi) - f(m,t)\beta(m,\phi)].\end{aligned} \tag{5}$$

Solving these equations with the initial conditions, $f(1,0)=1$ and $\phi(0)=\phi_0$, yields the evolution of the cluster size distribution as crystallization progresses. This requires knowledge of $\phi(t)$ and the average dissociation and aggregation rates, $\alpha(m,\phi)$ and $\beta(m,\phi)$.

For hard sphere suspensions the aggregation and dissociation rates have been determined previously [10,48] as follows. To determine dissociation rates, particles on a cluster surface are assumed to reside in potential energy wells because of their bonds with their nearest neighbors [10,49]. Although two hard sphere particles experience no interactions in dilute suspensions except for an infinite repulsion at contact, in dense suspensions, the prominent peak in the pair distribution function, $g(r)$, at contact indicates the tendency of two nearby hard sphere particles to come close to each other rather than stay separated [50]. This tendency is treated as an effective attraction between the particles that leads to bond formation. The strength of these bonds is estimated using the potential of mean force [10,50]. The number of these bonds, C_s, depends on the cluster radius, R, as $C_s(R) = C_f + (C_{s\infty} - C_f)(1 - \exp\{\zeta(R_{\min} - R)/2a\})$, and determines the depth of the potential well in which the surface particles reside. Here, C_f is the number of nearest neighbors of a particle in the fluid, which, following previous estimates, is set at 9 over the volume fraction range of interest [10]. $C_{s\infty} = 11$ is the number of nearest neighbors of a particle on the surface of an infinitely large cluster, and its value is determined from conditions enforcing thermodynamic consistency [10]. $R_{\min} = a(2/0.74)^{1/3}$ is the radius of the smallest possible cluster, i.e., containing two particles. The form for $C_s(R)$ chosen here is an empirical interpolation, where the parameter ζ controls the rate of increase of C_s from C_f to $C_{s\infty}$ as R increases [10]. This parameter can, in principle, be determined independently. In addition, it is related to the curvature dependence of the solid-fluid surface tension as discussed below.

The motion of the particles in this potential well is described by the Smoluchowski equation [48]. Solving the Smoluchowski equation, the average time required for the particles to diffuse out of their potential wells into the bulk suspension is determined. Then, the rate at which particles dissociate from the cluster surface is

$$\alpha(m,\phi)=\begin{cases}\dfrac{6\omega D_0\phi_R R}{a^3}\dfrac{[1-(1-a/R)^3]}{[1-a/2R]}\dfrac{[1+a/R]^2}{[(1+a/R)^3-1]}\left[\dfrac{(1-\phi_R)^3}{(1-\phi_R/2)}\right]^{C_s-C_f}, & m>1,\\ 0, \quad m=1\end{cases} \tag{6}$$

where the clusters are assumed to be spherical, so that $m=(R/a)^3\phi_{\text{cryst}}$. The packing fraction of particles on the surface, $\phi_R=0.486+0.154\exp\{\xi(\phi-0.64)/(\phi-\phi_s)\}$, and $\phi_s=0.495$ is the solubility boundary for hard sphere suspensions [10]. Again, the form for ϕ_R is an empirical interpolation where the parameter ξ characterizes how the density of particles in the surface layer changes with the suspension volume fraction. We relate this parameter to the volume fraction dependence of the solid fluid surface tension as discussed below. D_0 is the Stokes-Einstein diffusivity of the particles, and $\omega=0.2$ is an approximate hydrodynamic correction to D_0 on the cluster surface [10].

As particles associate to form clusters, a small zone around the clusters becomes depleted of monomers. This generates a gradient in the concentration of monomers from the bulk suspension to the cluster surfaces. Particles are assumed to aggregate onto cluster surfaces by diffusing down this concentration gradient. Knowing the gradient diffusivity of hard sphere particles, the diffusion equation is solved to give the aggregation rate as [10]

$$\beta(m,\phi)=\frac{3RD_0}{a^3}\left(1+\frac{a}{R}\right)\int_{\phi_R}^{\phi}(1-\phi')^{2.55}(1+4\phi'+4\phi'^2-4\phi'^3+\phi'^4)d\phi'. \tag{7}$$

To determine $\phi(t)$, we assume that all clusters exist in mechanical equilibrium with the background suspension [10]. For determining nucleation rates and induction times, we are interested in the evolution of the system over times small compared to the times over which crystallization reaches completion. At these short times, Harland and van Megen [13] showed that crystals exist in mechanical equilibrium with the background suspension for $\phi_0>\phi_m$. Here, we assume the approximation to hold for $\phi_0<\phi_m$ as well. Then, by equating the pressures in the solid and fluid phases using the known equations of state for the two phases [51,52], ϕ_{cryst} can be related to ϕ as follows [10]:

$$\phi_{\text{cryst}}=\frac{0.738}{1+\dfrac{2.17(1-\phi)^3}{(1+\phi+\phi^2-\phi^3)\phi}}. \tag{8}$$

From ϕ_{cryst} and $f(1,t)$, the volume occupied by the clusters is determined. Assuming the total volume of the crystallizing sample to be fixed, this gives the volume available for the monomers in the background suspension. Then, knowing the volume occupied by the monomers, $\phi(t)$ can be determined as

$$\phi(t)=\frac{\phi_0 f(1,t)}{1-\dfrac{\phi_0(1-f(1,t))}{\phi_{\text{cryst}}(\phi(t))}}. \tag{9}$$

Equation (9) closes the set of coupled differential population balance equations, represented by Eqs. (5)–(8) above, which can now be solved to obtain the evolution of the cluster size distribution as crystallization progresses. We present our calculations and comparisons with experiments in the following section.

IV. MODEL CALCULATIONS AND COMPARISONS WITH EXPERIMENTS

A. Evolution of the cluster size distribution

Shown in Fig. 1 is the evolution of the cluster size distribution, $f(m,t)$, obtained by integrating the population balance equations, Eqs. (5)–(9), for a hard sphere suspension with $\phi_0=\phi_m=0.55$. (For these calculations, the values $\zeta=0.9$ and $\xi=1.0$ have been used and will be explained below.) Beginning with $f(m,0)$ as a δ function at $m=1$, $f(m,t)$ increases with time for $m>1$ and decreases for $m=1$. The monotonic decrease of $f(1,t)$ indicates the conversion of monomers to larger clusters. For $m>1$, $f(m,t)$ first increases, reaches a maximum value, $f^{\max}(m,t^{\max})$, at which it stays for an extended period of time and eventually decreases. $t_{\max}$ increases monotonically with m. We note that similar trends, where the number densities of clusters of increasing sizes sequentially reach steady states, have been predicted by Shi and Sienfeld [44].

The corresponding evolution of the monomer volume fraction, $\phi(t)$, is shown in Fig. 2 for several values of ϕ_0. Three distinct regimes characterize the evolution of $\phi(t)$: a sharp initial decrease, an intermediate plateau, where $\phi\approx\phi_{\text{plat}}(\phi_0)$, and a late third regime of less rapid decrease. The existence of these regimes leads to the following description of the nucleation process.

In a metastable suspension consisting of monomers alone, pairs of monomers aggregate to form dimers. When $m^*\gg 2$, dimers have a much greater tendency to shrink than to grow. As a result, a pseudo-steady-state distribution is quickly established between monomers and dimers. Accordingly, ϕ decreases from ϕ_0 to ϕ_{plat}. Slowly, however, trimers form, and the distribution shifts to a steady state between monomers, dimers, and trimers. As the number density of trimers is small $[f(3,t)/f(2,t)\ll 1]$, ϕ remains nearly constant at ϕ_{plat}. This process continues, with bigger clusters forming at increasingly slower rates, until clusters of the critical size are formed. These clusters have a greater tendency to grow than to shrink. As they grow, monomers are

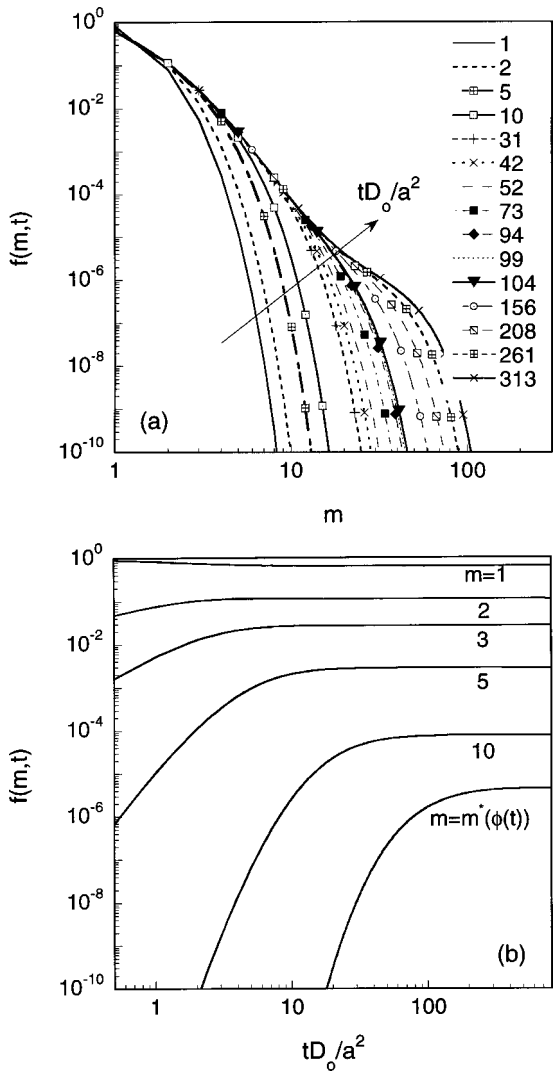

FIG. 1. Time evolution of the cluster size distribution, obtained by solving Eqs. (5)–(9), in a suspension with an initial monomer volume fraction, $\phi_0 = 0.55$.

rapidly consumed from the background suspension driving ϕ below ϕ_{plat}.

Based on this description, a good estimate of ϕ_{plat} can be obtained from a steady state distribution of monomers and dimers alone. This yields

$$\phi_{\text{plat}} = \frac{\phi_0}{1 + \dfrac{2\beta(1,\phi_{\text{plat}})}{\alpha(2,\phi_{\text{plat}})}\left[1 - \dfrac{\phi_0}{\phi_{\text{cryst}}(\phi_{\text{plat}})}\right]}. \qquad (10)$$

As shown in Fig. 3, estimates of ϕ_{plat} obtained thus are in excellent agreement with the values obtained from solving the population balance equations. The slightly but systematically higher values of ϕ_{plat} obtained from Eq. (10) suggest the presence of small numbers of larger clusters as expected. The rapid reduction of the background monomer volume fraction during crystallization significantly reduces the driving force for nucleation. Nucleation occurs at a rate determined by $\phi \sim \phi_{\text{plat}}$ and not ϕ_0 as assumed in classical models.

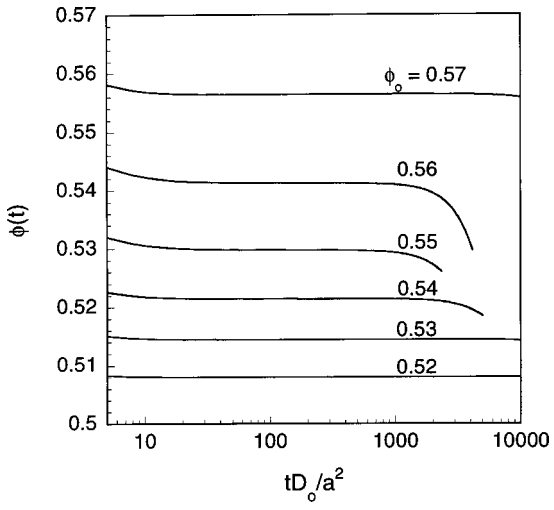

FIG. 2. Time evolution of the background monomer volume fraction, ϕ, for different values of ϕ_0.

B. Nucleation rates, growth rates, and induction times

Measurements of nucleation rates during the crystallization of hard sphere suspensions have been reported by several groups [12–14,30]. Simulation studies have also been performed [9], and classical [13,14,28,35,49] and kinetic [10] models have been applied to interpret the experiments and simulations. While significant quantitative discrepancies exist, the following qualitative trends have been observed: At small supersaturations, as ϕ increases above ϕ_s, the thermodynamic driving force for crystallization increases, resulting in an increase in nucleation rates. At very high volume fractions, however, the concentration gradient between the surface of a crystal nucleus and the bulk suspension diminishes. Aggregation of particles onto the crystal surface, being driven by gradient diffusion, also diminishes, reducing the nucleation rate. As a result of these competing influences, a maximum in the nucleation rate occurs at an intermediate volume fraction of about 0.56.

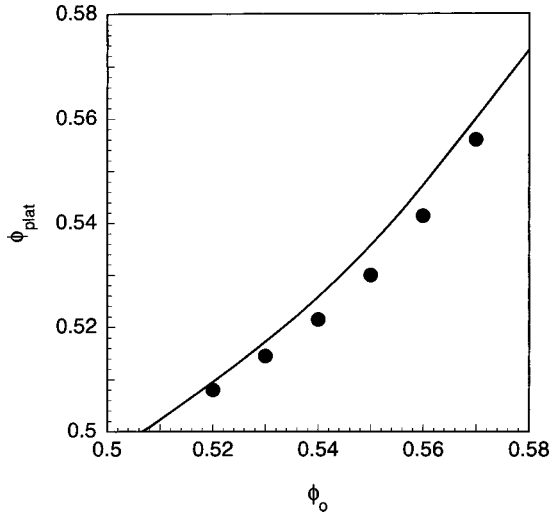

FIG. 3. Intermediate plateau volume fractions (see text), ϕ_{plat}, for different values of ϕ_0. The solid line represents calculations via Eq. (10) and the symbols are obtained by solving Eqs. (5)–(9).

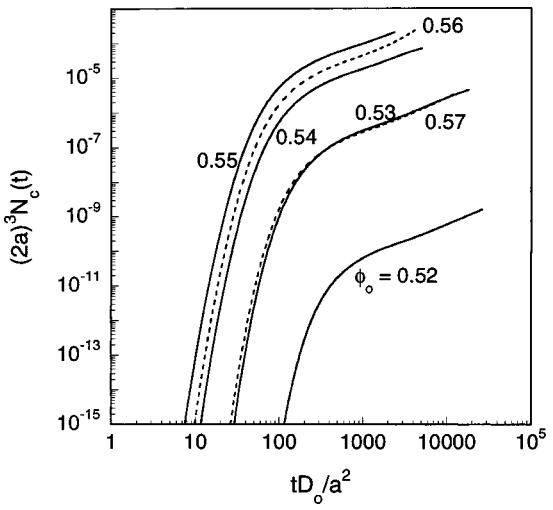

FIG. 4. Time evolution of the number of crystals for different values of ϕ_0, calculated using Eq. (3).

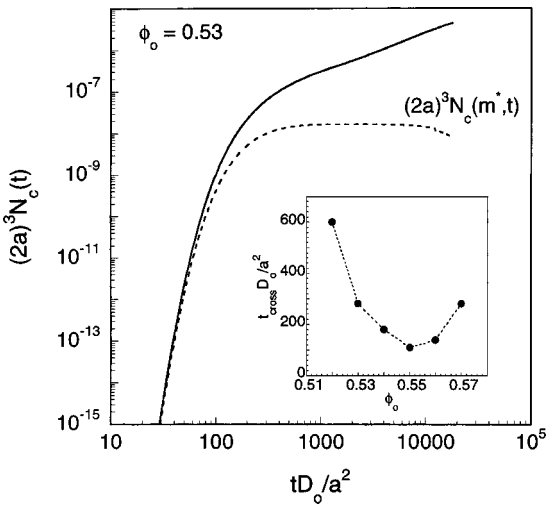

FIG. 5. Time evolution of the total number of crystals (solid line) compared with that of the number of crystals of the critical size (dashed line) for $\phi_0=0.53$. The inset shows the crossover time (see text), t_{cross}, as a function of ϕ_0.

Steady state nucleation rates predicted by the classical approach capture the experimental data well, albeit using the solid fluid surface tension (or another quantity such as the particle diffusivity) as an adjustable parameter [9,10,13,14,49]. In the classical approach, ϕ is assumed to remain constant at ϕ_0 during crystallization. From the population balance model above, however, we note that ϕ quickly decreases to ϕ_{plat}. At the same time, the analyses of the experimental estimates in Sec. II show that the experimentally determined $J(t)$ measures a different quantity from that predicted by classical models. Employing classical models for analyzing data from scattering experiments is therefore questionable. Here, we employ the population balance model to calculate experimental quantities as described in Sec. II.

We begin in Fig. 4 with calculations of the number of crystals, $N_c(t)$, using Eq. (3), for several values of ϕ_0. The parameter values $\zeta=0.9$ and $\xi=1.0$ are used (see below). At small times $N_c(t)$ increases rapidly, followed by a regime of much slower increase. The two regimes are understood by comparing $N_c(t)$ to the quantity $N_c(m^*,t)=(1/8a^3)[\phi_0/\phi_{\text{cryst}}(t)]f(m^*,t)$, which is the contribution of the number of critical clusters to $N_c(t)$, as shown in Fig. 5 for $\phi_0=0.53$. We note that up to the crossover from the first to the second regime, which occurs at a time we denote $t_{\text{cross}}(\phi_0)$, $N_c(t)\approx N_c(m^*,t)$. Beyond t_{cross}, $N_c(t)$ continues to increase, whereas $N_c(m^*,t)$ stays constant for a substantial period of time and then decreases. Thus, t_{cross} characterizes the time for the cluster size distribution up to the critical size to reach steady state and is closely related to the lag time predicted by classical models [5,42–46]. In the inset of Fig. 5, we show t_{cross} as a function of ϕ_0.

In Fig. 6, we present calculations of time dependent nucleation rates, $J(t)$, using Eq. (4), for different values of ϕ_0. Since changes in $N_c(t)$ are over several orders of magnitude, we simplify Eq. (4) using $dN_c(t)/dt\sim N_c(t)/t$. For all values of ϕ_0, we find that $J(t)$ first rises sharply until $t\sim t_{\text{cross}}(\phi_0)$. Beyond t_{cross}, $J(t)$ rises more slowly and reaches a plateau value $J_{\text{plat}}(\phi_0)$ before decreasing eventually. Thus, as predicted by classical models and as observed in experiments, $J(t)$ appears to attain a pseudo-steady-state value after a transient period.

In Fig. 7, we compare our calculations of $J_{\text{plat}}(\phi_0)$ with the experimental estimates of Palberg [14], Schatzel and Ackerson [29], and Harland and van Megen [13], and the simulation data of Auer and Frenkel [9]. We find good agreement between our predictions and the experimental estimates. Our predictions capture the qualitative trends of the experiments accurately. Quantitative discrepancies of several orders of magnitude exist between independent experimental estimates, and between experiments and simulations. The origins of these discrepancies remain poorly understood. One reason for the discrepancies might be that the simulations of Auer and Frenkel [9] employ approximate descriptions of the hydrodynamic interactions of the colloidal particles in suspension. Our predictions agree with the experimental estimates to within the uncertainties in the experiments.

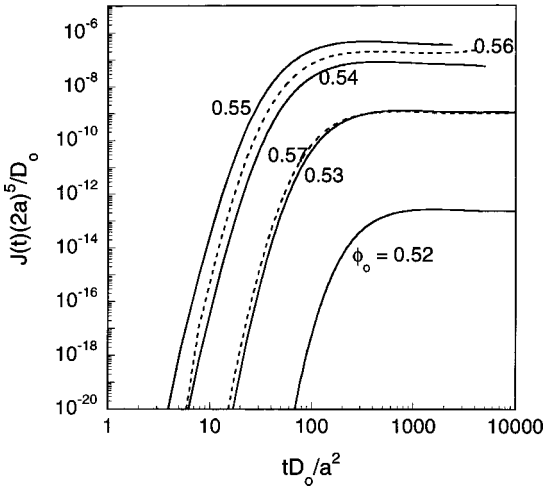

FIG. 6. Time dependent nucleation rates calculated via Eq. (4) for several values of ϕ_0.

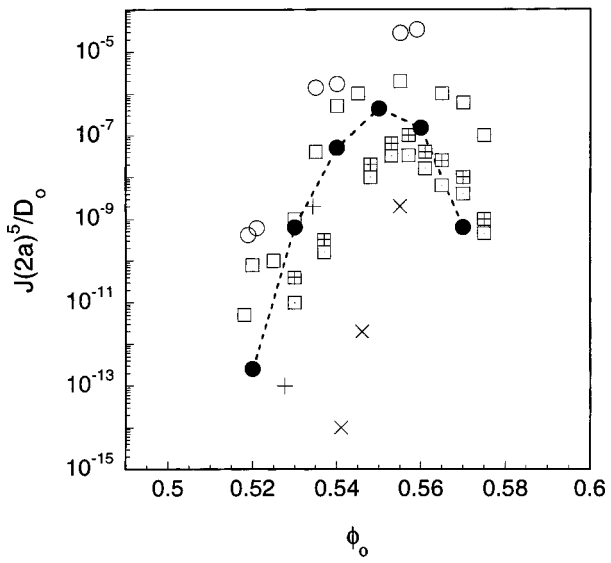

FIG. 7. Pseudo-steady nucleation rates (the plateau values in Fig. 6) as a function of ϕ_0 (filled circles) compared to the experimental estimates from Palberg [14] (open squares), Schatzel and Ackerson [29] (circles), maximum (checkered squares) and average (dotted squares) nucleation rates from Harland and van Megen [13], and from the simulations of Auer and Frenkel [9] of monodisperse (+) and polydisperse (×) hard sphere suspensions.

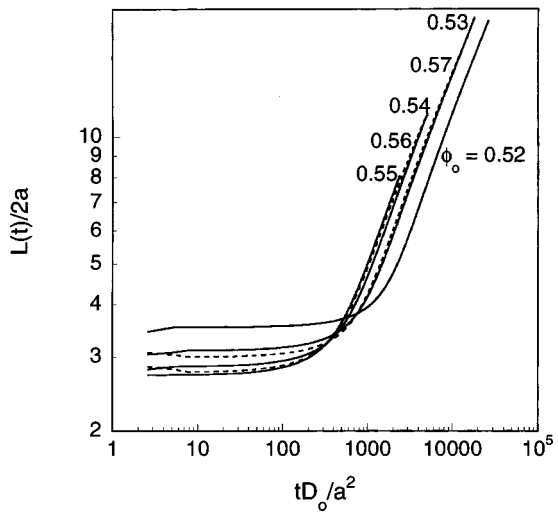

FIG. 8. Time evolution of the average crystal size calculated using Eq. (1) for several values of ϕ_0 showing the t^0 dependence at short times and the $t^{1/2}$ dependence at long times.

The parameters ζ and ξ are associated with the volume fraction at the cluster liquid interface and the cluster size dependence of the number of nearest neighbors. These parameters can be linked to the curvature and the volume fraction dependence, respectively, of the solid fluid surface tension, γ, as follows [10]:

$$\frac{\gamma(R,\phi)a^2}{kT} = \frac{\phi_R R}{4\pi a}\frac{(1-(1-a/R)^3)}{(1-a/2R)}[C_{\text{cryst}}\ln g(2a,\phi_{\text{cryst}}) - C_s \ln g(2a,\phi_R)], \tag{11}$$

where $C_{\text{cryst}}=12$, $\phi_R=0.486+0.154\exp\{\xi(\phi-0.64)/(\phi-\phi_s)\}$, and $\phi_s=0.495$, $C_s=C_f+(C_{s\infty}-C_f)\exp[\zeta(R_{\min}-R)/2a]$, and $g(2a,\phi)=(1-\phi/2)/(1-\phi)^3$. Thus, knowing the curvature and volume fraction dependence of γ, the parameters ζ and ξ can be determined independently. Such information for hard sphere crystals is not available. As a result, we treat the parameters as adjustable and choose the values $\zeta=0.9$ and $\xi=1.0$, to yield the best agreement between predictions of $J_{\text{plat}}(\phi_0)$ and experimental nucleation rates.

Because nucleation rates attain pseudo-steady-state values, classical treatments, assuming ϕ to be constant, can be applied to predict the experimental nucleation rates. As shown previously, such approaches lead to a different set of values for ζ and ξ [10]. Differences in the parameter values correspond to differences in γ. In particular, for $R \gg a$ and $\phi \approx 0.55$, $\gamma a^2/kT=0.23$ when $\zeta=0.9$ and $\xi=1.0$, whereas $\gamma a^2/kT=0.20$ as determined previously [10]. This suggests that fits to experimental estimates of nucleation rates assuming ϕ remains constant at ϕ_0 result in smaller values of γ than their true values. This is in agreement with the conclusion of Auer and Frenkel [9], who find that the values of γ obtained from such fits ($\gamma a^2/kT \approx 0.12$) are lower than those obtained from fits to their simulation data ($\gamma a^2/kT \approx 0.18$). Note that classical nucleation theory predicts nucleation rates to be proportional to $\exp(A\gamma^3)$, where A is a constant at a given supersaturation so that the rates are exceptionally sensitive to changes in γ. Interestingly, however, we find that predictions of steady state nucleation rates using the classical approach [10] (not shown) with the parameter values $\zeta=0.9$ and $\xi=1.0$ but using ϕ_{plat} instead of ϕ_0 compare quite well with the experiments.

To compare crystal growth rate data with model predictions, we present in Fig. 8 calculations of $L(t)$ using Eq. (1) for several values of ϕ_0. Again, two distinct regimes characterize the evolution of $L(t)$, separated by $t_{\text{cross}}(\phi_0)$. $L(t)$ is nearly independent of t for $t<t_{\text{cross}}$, and begins to rise for $t>t_{\text{cross}}$ with a power law dependence on t. The behavior for $t<t_{\text{cross}}$ is consistent with the fact that in this regime the number of clusters of the critical size increases tremendously, whereas the number of bigger clusters remains almost constant. Therefore, $L(t<t_{\text{cross}}) \sim [m^*(\phi_{\text{plat}}(\phi_0))]^{1/3}$, and is almost constant. For $t>t_{\text{cross}}$, we find that $L(t) \sim t^{1/2}$, for all ϕ_0. Both these dependences have been observed in experiments and have been predicted by the recent analysis of Cheng *et al.* [36]. In Fig. 9, we compare experimental growth rate data with the predictions of Eq. (1). The comparisons are quite satisfactory indicating that the population balance model captures much of the behavior observed experimentally during the nucleation and growth of hard sphere crystals. [We note that the model for crystal growth in Ref. [10] using $\phi(t)=\phi_0$ predicts the $t^{1/2}$ dependence for long times but fails to predict the t^0 dependence for small times. This is due to its inability to predict the growth of subcritical clusters. As a result, experimental values of L ($>R^*$) and t were employed as inputs for calculating growth rates, resulting in the apparent better agreement between model predictions and experiments.]

Finally, we present comparisons of measured and calcu-

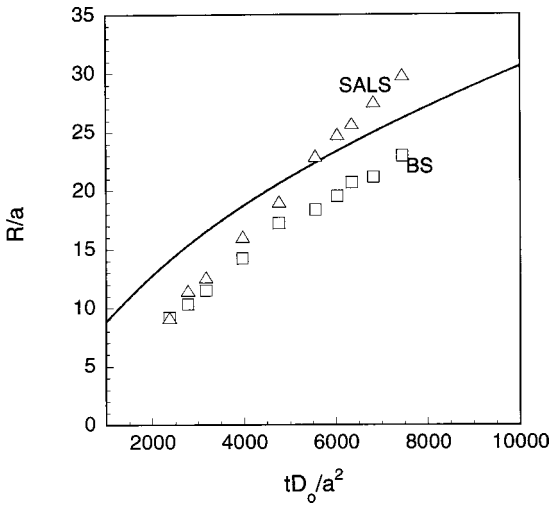

FIG. 9. Time evolution of the average crystal sizes calculated using Eq. (1) for $\phi_0=0.535$ (solid line), compared with the experimental estimates of Palberg [14] obtained via small angle light scattering (triangles) and Bragg scattering (squares) also for $\phi_0=0.535$.

lated induction times during hard sphere crystallization. We emphasize that due to the inability of previous attempts to predict the evolution of cluster size distributions and the failure to link measured and predicted quantities, no models currently exist to predict induction times. The present comparison is only possible because the model is developed to predict the evolution of cluster size distributions, $f(m,t)$, and thus provides a rigorous test of model predictions.

The time evolution of the fraction of the sample crystallized, $X(t)$, calculated using Eq. (2), is presented in Fig. 10 for several values of ϕ_0. $X(t)$ counts clusters bigger than the critical cluster size, m^*, and is small during the rapid formation of smaller clusters in the initial stage of nucleation. As the number of clusters bigger than m^* increases, $X(t)$ increases and yields an induction time determined as shown. In

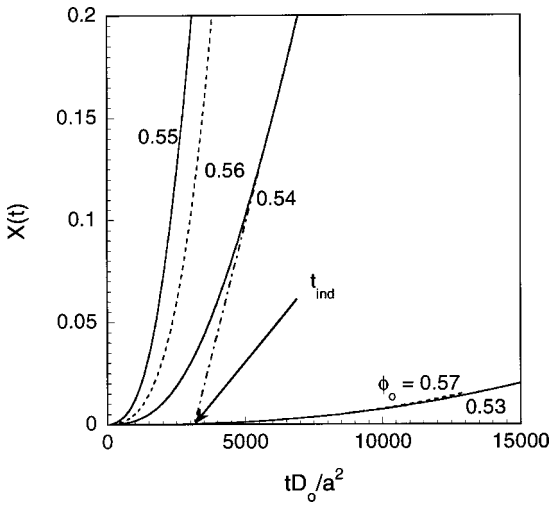

FIG. 10. Time evolution of the fraction of the suspension crystallized calculated using Eq. (2) for several values of ϕ_0. The procedure for calculating $t_{\rm ind}$ is demonstrated for $\phi_0=0.54$.

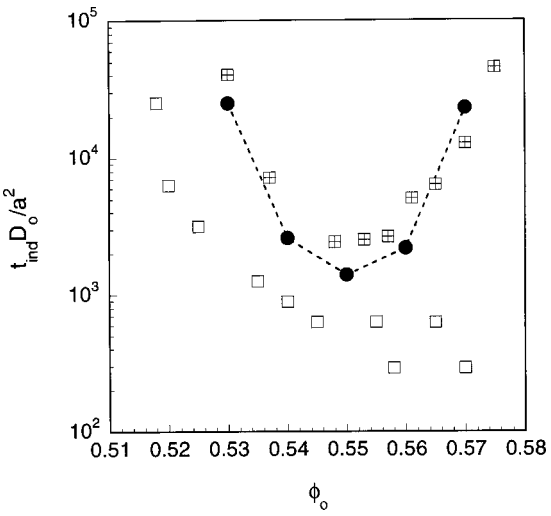

FIG. 11. Induction times calculated using Eq. (2) (circles) (see text) and compared with the experimental estimates of Harland and van Megen [13] (checkered squares) and Palberg [14] (open squares).

Fig. 11, we present calculations of the induction times and compare them with the experimental estimates of Harland and van Megen [13] and Palberg [14], both obtained from Bragg scattering experiments. We note that a qualitative discrepancy exists in the ϕ_0 dependence of the induction times, $t_{\rm ind}$, reported in the two experimental data sets. As ϕ_0 is increased up to 0.55, $t_{\rm ind}$ decreases and the two data sets agree to within an order of magnitude. Beyond $\phi_0=0.55$, however, $t_{\rm ind}$ increases in the estimates of Harland and van Megen, whereas it continues to decrease monotonically according to Palberg. The origins of this discrepancy remain poorly understood. Our model agrees qualitatively with the estimates of Harland and van Megen, predicting a minimum in $t_{\rm ind}$ at $\phi_0\sim0.55$. Quantitatively as well, our model captures the data of Harland and van Megen to within an order of magnitude.

The ability of our model to predict induction times is a significant advantage over classical models. Direct measurements of nucleation rates are difficult and more reproducible induction time measurements are often used to estimate nucleation rates. More recent applications involving protein crystallization preclude nucleation rate measurements from scattering experiments, as the particle sizes are significantly smaller than the wavelength of light. Here, small angle light scattering experiments allow induction time measurements, but their interpretation is confounded by the lack of models [24,25]. The present model thus provides a route to extract valuable information from such experiments.

V. CONCLUSIONS

The population balance model presented here predicts the time evolution of the cluster size distribution during crystallization and allows us to predict quantities that are measured experimentally to probe the kinetics of colloidal crystallization. In particular, comparisons have been made between predicted and measured nucleation rates, crystal growth ve-

locities, and induction times, the measurements made via light scattering experiments on the crystallization of hard sphere suspensions. Model calculations suggest that predictions of these quantities are affected significantly by the decrease in the background monomer volume fraction as crystallization progresses. Classical approaches assume the background monomer volume fraction to remain fixed, and therefore, overestimate the driving force for crystallization. At the same time, discrepancies exist in the definitions of the quantities predicted by classical models and the quantities measured experimentally. Consequently, fits using the classical approaches to experimental estimates of nucleation and growth rates result in erroneous values of the adjustable parameters like the solid-fluid surface tension. The kinetic model presented here predicts the evolution of the cluster size distribution during crystallization, and accounts explicitly for these effects. In addition, a significant advantage over classical models is the ability of the population balance model to predict induction times. Measurements of induction times are much simpler than nucleation rates, but interpreting the resulting data has been confounded by the lack of models. Predictions of induction times using the kinetic model compare well with experiments.

ACKNOWLEDGMENTS

The authors acknowledge support from the U.S. DOE via the University of Illinois at Urbana Champaign, Frederick Seitz Materials Research Laboratory Grant No. DEFG02-96ER45439. Insightful discussions with Professor Richard Braatz and his group are also gratefully acknowledged.

[1] A. McPherson, *Preparation and Analysis of Protein Crystals* (Kreiger, Florida, 1982).
[2] P. V. Braun and P. Wiltzius, Nature (London) **402**, 603 (1999).
[3] P. Tessier, O. D. Velev, A. T. Kalambur, A. M. Lenhoff, J. F. Rabolt, and E. W. Kaler, Adv. Mater. **13**, 396 (2001).
[4] R. Becker and W. Doring, Ann. Phys. (Leipzig) **24**, 719 (1935).
[5] P. G. Debenedetti, *Metastable Liquids: Concepts and Principles* (Princeton University Press, Princeton, NJ, 1996).
[6] D. W. Oxtoby, J. Phys.: Condens. Matter **4**, 7627 (1992).
[7] P. E. Wagner and R. Strey, J. Phys. Chem. **85**, 2694 (1981).
[8] N. M. Dixit, A. M. Kulkarni, and C. F. Zukoski, Colloids Surf., A **190**, 47 (2001).
[9] S. Auer and D. Frenkel, Nature (London) **409**, 1020 (2001).
[10] N. M. Dixit and C. F. Zukoski, Phys. Rev. E **64**, 041604 (2001).
[11] J. Deubener and M. C. Weinberg, J. Non-Cryst. Solids **231**, 143 (1998).
[12] U. Gasser, E. R. Weeks, A. Schofield, P. N. Pusey, and D. A. Weitz, Science **292**, 258 (2001).
[13] J. L. Harland and W. van Megen, Phys. Rev. E **55**, 3054 (1997).
[14] T. Palberg, J. Phys.: Condens. Matter **11**, R323 (1999).
[15] D. F. Rosenbaum and C. F. Zukoski, J. Cryst. Growth **169**, 752 (1996).
[16] D. F. Rosenbaum, P. C. Zamora, and C. F. Zukoski, Phys. Rev. Lett. **76**, 150 (1996).
[17] N. Asherie, A. Lomakin, and G. B. Benedek, Phys. Rev. Lett. **77**, 4832 (1996).
[18] N. M. Dixit and C. F. Zukoski, J. Colloid Interface Sci. **228**, 359 (2000).
[19] A. M. Kulkarni and C. F. Zukoski (unpublished).
[20] A. Lomakin, N. Asherie, and G. B. Benedek, Proc. Natl. Acad. Sci. U.S.A. **96**, 9465 (1999).
[21] R. P. Sear, J. Chem. Phys. **111**, 4800 (1999).
[22] M. Hloucha, J. F. M. Lodge, A. M. Lenhoff, and S. I. Sandler, J. Cryst. Growth **232**, 195 (2001).
[23] B. Biscans and C. Laguerie, J. Phys. D **26**, B118 (1993).
[24] A. M. Kulkarni and C. F. Zukoski, J. Cryst. Growth **232**, 156 (2001).
[25] T. E. Paxton, A. Sambanis, and R. W. Rousseau, Langmuir **17**, 3076 (2001).
[26] J. K. G. Dhont, C. Smits, and H. N. W. Lekkerkerker, J. Colloid Interface Sci. **152**, 386 (1992).
[27] O. Sohnel and J. W. Mullin, J. Colloid Interface Sci. **123**, 43 (1988).
[28] B. J. Ackerson and K. Schatzel, Phys. Rev. E **52**, 6448 (1995).
[29] K. Schatzel and B. J. Ackerson, Phys. Rev. E **48**, 3766 (1993).
[30] J. Zhu, M. Li, R. Rogers, W. Meyer, R. H. Ottewill, W. B. Russel, and P. M. Chaikin, Nature (London) **387**, 883 (1997).
[31] D. Z. Cheng, W. B. Russel, and P. M. Chaikin, Nature (London) **401**, 893 (1999).
[32] D. J. W. Aastuen, N. A. Clark, L. K. Cotter, and B. J. Ackerson, Phys. Rev. Lett. **57**, 1733 (1986).
[33] Y. He, B. J. Ackerson, W. van Megen, S. M. Underwood, and K. Schatzel, Phys. Rev. E **54**, 5286 (1996).
[34] K. E. Davis and W. B. Russel, Ceram. Trans. **1B**, 693 (1988).
[35] W. B. Russel, P. M. Chaikin, J. Zhu, W. V. Meyer, and R. Rogers, Langmuir **13**, 3871 (1997).
[36] Z. Cheng, J. Zhu, W. B. Russel, W. V. Meyer, and P. M. Chaikin, Appl. Opt. **40**, 4146 (2001).
[37] Y. He and B. J. Ackerson, Physica A **235**, 194 (1997).
[38] S. Derber, T. Palberg, K. Schatzel, and J. Vogel, Physica A **235**, 204 (1997).
[39] B. J. Alder and T. E. Wainwright, J. Chem. Phys. **27**, 1208 (1957).
[40] W. B. Russel, D. A. Saville, and W. R. Schowalter, *Colloidal Dispersions* (Cambridge University Press, Cambridge, 1989).
[41] P. N. Pusey and W. van Megen, Phys. Rev. Lett. **59**, 2083 (1987).
[42] D. T. Wu, J. Chem. Phys. **97**, 2644 (1992).
[43] V. A. Schneidman and M. C. Weinberg, J. Chem. Phys. **97**, 3621 (1992).
[44] G. Shi and J. H. Seinfeld, Phys. Rev. A **41**, 2101 (1990).
[45] K. F. Kelton, Acta Mater. **48**, 1967 (2000).
[46] A. F. Izmailov, A. S. Myerson, and S. Arnold, J. Cryst. Growth **196**, 234 (1999).
[47] R. W. James, in *Optical Principles of the Diffraction of X-Rays*, edited by L. Bragg (Cornell University Press, Ithaca, NY, 1965).

[48] G. Narasimhan and E. Ruckenstein, J. Colloid Interface Sci. **128**, 549 (1989).
[49] W. B. Russel, Phase Transitions **21**, 127 (1990).
[50] D. A. McQuarrie, *Statistical Mechanics* (Harper and Row, New York, 1976).
[51] N. F. Carnahan and K. E. Starling, J. Chem. Phys. **51**, 635 (1969).
[52] K. R. Hall, J. Chem. Phys. **57**, 2252 (1972).